A Model for Relations between Needle Deflection, Force, and Thickness on Needle Penetration

Hiroyuki Kataoka[1], Toshikatsu Washio[2], Michel Audette[2], and Kazuyuki Mizuhara[3]

[1] NEDO Industrial Technology Researcher, Surgical Assist Technology Group, National Institute of Advanced Industrial Science and Technology(AIST)
[2] Surgical Assist Technology Group, National Institute of Advanced Industrial Science and Technology(AIST)
[3] Dept. of Mechanical Engineering, Tokyo Denki University

Abstract. A force-deflection model of needle penetration is proposed and evaluated experimentally. The force at the fixed end of the needle and the needle deflection were measured using a force sensor and a bi-plane X-ray imaging system, and the model was evaluated with the data. We define a physical quantity ω, which we call infinitesimal force per length, analogous to traction (force per surface area). The model predicts ω to be constant over the length of the inserted portion of the needle. However the results indicate that this assumption does not fully account for the real deflection. It is strongly suggested that there is an additional degree of freedom: a moment or a rotational force acting on the needle.

1 Introduction

Needle penetration is one of the least invasive treatments and some surgical robots are designed for this treatment [1]. However, it is known that it is not easy for surgeons to precisely reach the planned target inside soft tissue with a needle because a thin needle can be deflected in the tissue and the tissue itself also can be deformed by the needle, even if surgeons attempt to lead the needle in a straight direction. This problem makes the needle path planning difficult, and finally surgeons have to repeat the penetration by trial-and-error. Therefore clarifying the dynamics of both needle deflection and soft tissue deformation is expected to contribute to more efficient treatment through the precise planning of needle penetration with the help of preoperative simulation.

In order to model the tissue deformation and needle deflection, the relation between the locally applied force and motion of both the tissue and the needle have to be measured. However, there is no way to measure the local force directly since force sensors can only detect the force at their attached point, and it is also difficult to measure the local motion with enough temporal resolution. CT and MRI provide excellent 3D images, but these images are insufficient in both space and time resolution. Therefore we propose a new method of estimating the local force and

W. Niessen and M. Viergever (Eds.): MICCAI 2001, LNCS 2208, pp. 966-974, 2001.

motion of the needle based on the mechanical analysis of both the needle deflection and the force.

In order to achieve this estimation, a force-deflection model of a needle is required. There are some reports about needle force and deflection in the field of anesthesia [2-3]. Dentists have also reported significant needle deflection in dental anesthesia [4]. Though these reports measured the deflection of commercial needles corresponding to their length in the tissue in different gauges, tip types and target materials, they didn't investigate the relation between the force and the deflection of the needle. In addition, since the diameter of commercial needles is non-linear in gauge representation and the wall thickness of needles is different for product companies, the results in the reports cannot be compared quantitatively. Brett [5] measured the axial component of the needle force to detect the epidural puncture. However, he didn't investigate the transverse force, which has a strong effect on the needle deflection.

For these reasons we simultaneously measured the needle deflection and the transverse force at the fixed end of the needle on penetration in regularized conditions. In order to observe the needle deflection, we introduced a bi-plane X-ray imaging system for its ability to observe the needle deflection in three-dimensions and for its superior resolution in space and time, in comparison with MRI and CT.

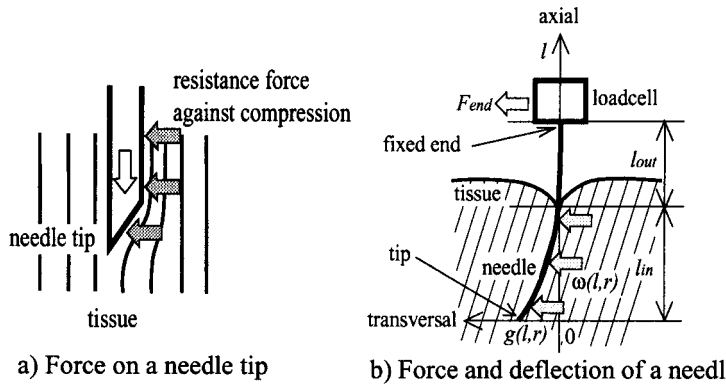

Fig. 1. A force-deflection model of a needle on penetration. $\omega(l,d)$ is the infinitesimal force per length on the needle side.

In this report we propose a novel force-deflection model: a needle with a bevelled tip goes forward while compressing the tissue around the tip, as shown in Fig.1a, and the needle is deflected by the resistance force against the compression. We introduce an assumption that the resistance force appears at the needle in a simple distribution (ie: with a constant direction everywhere along the length of inserted needle.) as shown in Fig.1b. The physical quantity used in the stress studies is the traction defined for a surface element as the limit of the surface force per area $\lim_{\Delta s \to 0} \Delta F_s / \Delta s$ [6]. However this quantity is less useful for a long thin shapes such as a needle, so we adopt the infinitesimal force per length $\omega = \lim_{\Delta l \to 0} \Delta F_l / \Delta l$, whereby ΔF_l is the force acting the segment of a curve, Δl is the length of short segment. From the transverse force at the fixed end F_{end}, measured by a three-axis loadcell, we can predict the

deflection $g(l,d)$ and the resistance force per length $\omega(l,d)$, as a function of axial position l and neelde diameter d. We evaluated the model by comparing the predicted deflection $g(l,d)$ and the measured deflection $\hat{g}(l,d)$. Since ω is supposed to be related to the volume of the inserted potion of the needle, which is the same as the volume of tissue displaced by the needle, the correlation between ω and the needle diameter is also investigated.

The study shows that the constant direction of ω assumed in the model does not fully account for the real deflection, and strongly suggest that there is an additional degree of freedom: a moment or rotational force acting on the needle.

2 Materials and Methods

2.1 Measurement of the Force to a Needle

We selected swine's hip muscle as a soft tissue penetration target. The skin was removed in order to simplify the needle behavior. A mass of muscle (200x200x70mm) was prepared from a slaughterhouse, whose size fully encompassed the tissue deformation caused by the penetration with a needle of 1mm diameter, the extent of which was determined in preliminary experiments.

The mass was laid on a flat styrene foam in the penetration machine as shown in Fig.2. The outside wall of the muscle was free.

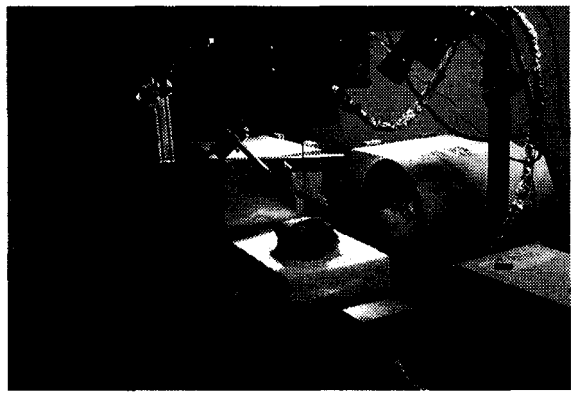

Fig. 2. A picture of the bi-plane X-ray imaging system. A sample muscle is on the penetration stage at the center.

A needle was located vertically above the center of the muscle, and both a three-axis loadcell (Nissho Co., 400N in axial and 100N in transverse direction is maximum) and a linear guide to drive the needle in its axial direction were attached at the fixed end of the needle. Some needles of different diameters (0.65mm, 1.00mm, 1.35mm, 1.55mm) were prepared. They were made from a solid cylindrical shaft to

simplify the influence of the tip shape. The needle tips were bevelled at an angle of 14 degrees to emphasize the deflection. Each needle was driven forward into the muscle at a constant speed of 5mm/sec, and stopped before the tip reached the tissue bottom. The output of the loadcell was recorded by a PC at the rate of 10Hz, 50Hz sampling followed by 5 sample averaging. The penetration was carried out twice for each needle, and the penetration point on the muscle was changed each time to prevent the needle from being inserted into the incision created by the previous penetration.

2.2 3D Reconstruction of the Needle Deflection from Stereo Images

Two sets of X-ray generators and detectors (EXM-60P, Toshiba IT & Control Systems Co.), whose maximum power is 60kv/1.2mA, were located diagonally around the muscle. The FOV of each X-ray is 40x30mm at the center of the penetration machine. Its imaging rate is 30 frames per second. To measure the three-dimensional needle deflection, the shape of the needle has to be reconstructed from the stereo images of the bi-plane X-ray system.

At first, the needle area in each image was extracted and skeletonized. Then the correspondences of the image coordinates of this skeletonized needle were checked with the following equation relating the stereo images [7]:

$$\boldsymbol{m}_a \boldsymbol{F} \boldsymbol{m}_b = 0 \tag{1}$$

where $\boldsymbol{m}_a$ and $\boldsymbol{m}_b$ are the image coordinates of the needle represented by the homogeneous coordinate system, and $\boldsymbol{F}$ is the fundamental matrix which is uniquely determined according to camera positions. In our system $\boldsymbol{F}$ can be determined as a unique matrix from preliminary X-ray calibration as X-ray generators and detectors are fixed. Once the correspondences were found, the 3D coordinates of the points comprising the needle were estimated by solving the following equations of a perspective camera model:

$$\lambda_a \boldsymbol{m}_a = \boldsymbol{P}_a \boldsymbol{x}_{3D} \tag{2}$$

$$\lambda_b \boldsymbol{m}_b = \boldsymbol{P}_b \boldsymbol{x}_{3D} \tag{3}$$

where $\boldsymbol{x}_{3D}$ represents the 3D coordinate of the needle in the homogeneous coordinate system, $\boldsymbol{P}_a$ and $\boldsymbol{P}_b$ are the perspective camera matrices which map the 3D coordinate system to the respective image coordinate systems. These matrices are also determined uniquely by X-ray calibration. Lastly λ_a and λ_b are arbitrary variables.

After the 3D coordinates of the needle were obtained, the deflection plane on which the needle mainly deflects was calculated to consider the deflection two-dimensionally. This plane is defined as being spanned by z and by the vector in the x-y plane, coinciding with the line regression of projections of the needle points on x-y plane as shown in Fig.3. Then the needle was projected on the deflection plane.

Finally, we consider the horizontal component of the loadcell output $F_{load\text{-}xy}$ and project it onto the deflection plane. We call this projection F_{end}, the transverse force at the fixed end of the needle.

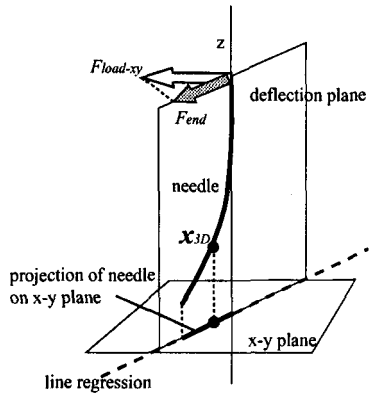

Fig. 3. The deflection plane on which the needle deflects. The plane is defined as being spanned by z and by the vector in the x-y plane, coinciding with the line regression of projections of the needle points on the x-y plane.

2.3 The Force-Deflection Model of a Needle

Following Fig.1 and [8], the needle deflection $g(l,d)$ caused by $\omega(l,d)$ can be described by solving the following equation:

$$\frac{d^2 g(l,d)}{dl^2} = -\frac{1}{EI}\int \omega(l,d)\, l\, dl \tag{4}$$

where l is the axial position of the needle whose origin is at the needle tip without deflection, E is Young's Modulus and I is the moment of inertia of the needle, d is the diameter of the needle. The transverse force at the fixed end of the needle F_{end} can be described as follows:

$$F_{end} = \int_0^{l_{in}} \omega(l,d)\, dl \tag{5}$$

where l_{in} is the insertion depth (refer to Fig.1b). By differentiating Eq.5 over l_{in}, ω can be represented as follows:

$$\frac{dF_{end}}{dl_{in}} = \omega(l,d) \tag{6}$$

We obtained w from F_{end} by Eq.6, and calculated the needle deflection by Eq.4 to compare with the real deflection.

To investigate the relation between ω and the needle diameter d, ω was plotted against d^2 as suggested by the dependence of the displaced tissue volume on the cross-sectional area.

3 Results

3.1 Measurement of the Force on the Needle

The transverse force at the fixed end of the needle is shown in Fig.4. The needles were penetrating the muscle during t=3 to t=10 seconds. Note that all curves show linear correspondence between the insertion depth and the force, as the penetration speed is constant therefore the time is linearly related with insertion depth in this time period. Also, note that the force remained constant after stopping the needle motion (t>10).

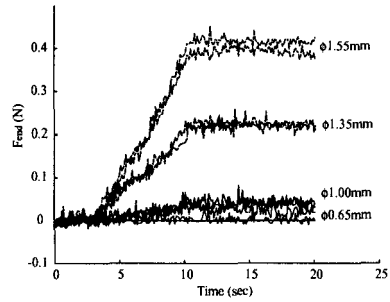

Fig. 4. The transverse force at the fixed end of the needle vs time for needles of different diameters. All needles stopped the penetration at t=10sec

3.2 3D Reconstruction of the Needle Deflection from Stereo X-ray Images

Figure 5 shows stereo images of a needle observed by the bi-plane X-ray imaging system. The gray area is the X-ray projection of the muscle, and the black line in the middle is the needle. The needle is deflected away from the vertical direction. The black dots in the muscle are the shadows of lead balls, which are used in tissue motion tracking research currently under way.

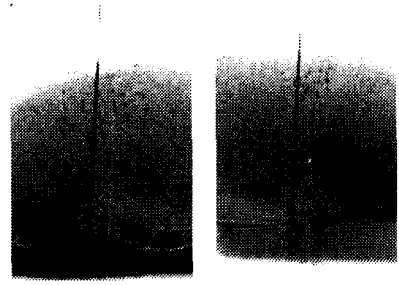

Fig. 5. Stereo X-ray images of a needle inside a mass of muscle. The gray area is the X-ray projection of the muscle, and the black line in the middle is the needle.

Figure 6 is the reconstructed deflection of the needles of different diameters on the deflection plane. The predicted and measured deflections as a function of l are linear and have comparable slopes, but differ by an offset (~2mm). This offset is explained by the model underestimating the deflection outside the tissue.

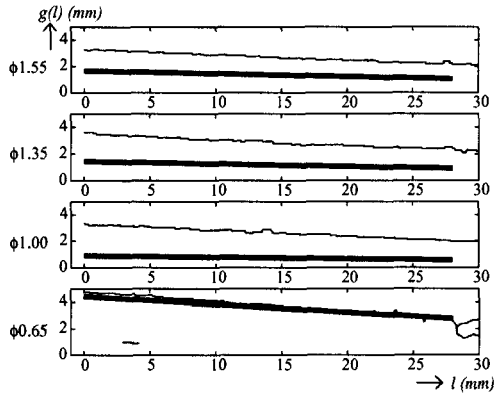

Fig. 6. The deflection of the measured and computed needles in different needle diameters. The thick lines are the computed deflection of the needle model, and the thin lines are the measured deflection of the real needle. The needle tip coincides with l=0mm, and the muscle surface is at l=28mm.

3.3 The Force-Deflection Model of the Needle

Figure 4 shows that the transverse force at the fixed end is proportional to the insertion depth. Hence, according to Eq.6, $\omega(l,d)$ can be defined as a constant value along the axial position of the needle. By defining this value as $W(d)$, the needle deflection can be now described as follows [8]:

$$g(l,d) = \frac{W(d)}{24EI}(l^4 - 4l_{in}(l_{in}^2 + 3l_{in}l_{out} + 3l_{out}^2)\, l + l_{in}(3l_{in}^3 + 12l_{in}^2 l_{out} + 18l_{in}l_{out}^2 + 8l_{out}^3)) \quad (0 \le l \le l_{in}) \tag{7}$$

where l_{out} is the length of the needle outside the tissue. The needle deflections calculated by Eq.7 are shown as thick lines in Fig.5, where E = 2.0x10^{2}GPa for stainless material, l_{in} = 28mm, l_{out} = 77mm. $W(d)$ is the value estimated from Fig.3 for each needle. The deflections of the reconstructed needles from X-ray images at the time the needles stopped are also shown in Fig.5 as thin lines.

The force per length $W(d)$ is plotted against the square of the needle diameter in Fig.7.

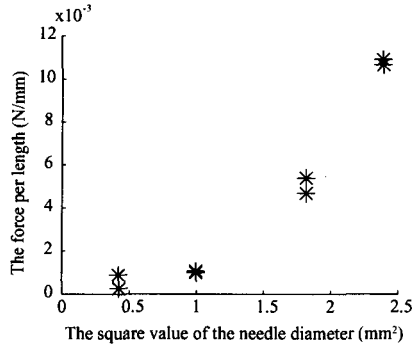

Fig. 7. The distribution forces to the square of the needle diameters (marked as *) and a regression line of the plots.

4. Discussion

4.1 Deflection Force

The transverse force at the fixed end in Fig.4 remained constant after the needle motion was stopped. This means that the origin of this force is not dynamic such as cutting force at the tip of the needle.

The transverse force Fend appeared proportional to the incremental insertion depth. This would imply that as insertion length increased the resistance force per length ω was constant, i.e., the incremental force from the tissue was constant regardless of the progress of needle deflection. However, an additional offset was caused by deflection outside the tissue ($g \neq 0$ at l=28), which the model underestimated as one can observe in Fig.6 at the muscle surface (l=28mm). This added deflection should cause ω to increase. Therefore, we need to consider other models of force distribution, resulting in ω varying with the insertion depth.

4.2 Model-Experiment Agreement

As shown in Fig.6 the predicted and measured deflections as a function of l are linear and have comparable slopes, but differ by an offset (~2mm). This offset is explained by the model underestimating the deflection outside the tissue.

In order to keep the same transverse force at the fixed end of the needle, the deflection offset $\left| \hat{g}(l,d) - g(l,d) \right|$ should be supplied by either an additional moment at the needle tip or a force per length, featuring a rotational component, whose integration is equal to the transverse force at the fixed end of the needle. We will try to apply the force-deflection model with this new ω in the next model.

4.3 Force per Length and Deflection vs Needle Diameter

Figure 7 suggests that the force per length increases with the needle diameter as the function of higher order than a quadratic function. This means that the variation of ω with needle size is not explained by only the variation of tissue volume displacement.

Finally, considering the real deflection values of the needle at 1.55, 1.35 and 1.00mm diameters which were similar to each other in Fig.6, there is a possibility that the needle deflection is determined only by the geometric factor such as the bevel angle of the needle tip.

5 Conclusions

The relation between the force on a needle and its deflection during needle puncture into biological tissue was investigated. A simple infinitesimal force per length relation was assumed as the force-deflection model and the predicted deflection was compared to the measured deflection. These showed a good agreement in the slope of the displacement vs length at different needle diameters. However, the predicted deflection was smaller than the measured deflection.

The transverse force at the fixed end was proportional to the needle length inside tissue, which would imply the constant force per length along the needle. However, the observed needle deflection exhibited a large component outside the tissue, which is incompatible with a constant force per length. Therefore, it is strongly suggested that an additional moment or rotational component is required.

References

1. Stoianovici, D., et.al., "An efficient needle injection technique and radiological guidance method for percutaneous procedures," In proc. of CRVMed-MRCAS '97, pp.295-298, 1997.
2. Sitzman, B.T.,et.al., "The effects of needle type, gauge, and tip bend on spinal needle deflection ," Anesth Analg, 82(2), pp. 297-301, 1996
3. Drummond, G.B., et.al., "Deflection of spinal needles by the bevel," Anaesthesia, 35(9), pp. 854-7, 1980
4. Robinson, S.F., et.al., "Comparative study of deflection characteristics and fragility of 25-, 27-, and 30-gauge short dental needles," JADA, 109, pp.920-924, 1984
5. Brett, P.N., et.al., "Schemes for the Identification of Tissue Types and Boundaries at the Tool Point for Surgical Needles," IEEE trans on Inf Technol Biomed, Vol.4, No.1, pp.30-36, 2000
6. Malvern, L.E., "Introduction to the Mechanics of a Continuous Medium," Prentice-Hall, Inc., New Jersey, 1969
7. Jun Sato, "Computer Vision - Geometry of Vision -," Corona Publishing Co. Ltd., Tokyo, 1999
8. JSME ed., "JSME Mechanical Engineers' Handbook," JSME, Tokyo, 1987